

Mechanistic study of apoptosis induced by high-fluence low-power laser irradiation using fluorescence imaging techniques

Shengnan Wu
Da Xing
Fang Wang
Tongsheng Chen

MOE Key Laboratory of Laser Life Science and
Institute of Laser Life Science
Guangzhou 510631, China

Wei R. Chen

MOE Key Laboratory of Laser Life Science and
Institute of Laser Life Science
Guangzhou 510631, China
and
College of Mathematics and Science
Department of Engineering and Physics
Biomedical Engineering Program
Edmond, Oklahoma 73034

Abstract. Low-power laser irradiation (LPLI) can cause cell proliferation, differentiation, or death; however, the cellular mechanisms of these effects of LPLI, at high or low fluences, are not well known. To investigate the mechanism of high-fluence LPLI-induced apoptosis, both human lung adenocarcinoma cells (ASTC-a-1) and African green monkey SV40-transformed kidney fibroblast cells (COS-7) were irradiated with a He-Ne laser for 10 min under a fluence of 120 J/cm² and 80 J/cm², respectively. The dynamics of reactive oxygen species (ROS) generation was determined by measuring changes in fluorescence resulting from oxidation of intracellular dichlorodihydrofluorescein diacetate (H₂DCFDA) to (DCF). The changes of mitochondrial membrane potential, $\Delta\Psi_m$, were studied by measuring the reduction of cellular fluorescence of Rhodamine 123 dyes using confocal laser scanning microscopy. The activation of caspase-3 in cells transfected by [SCAT3] reporters was observed using fluorescence resonance energy transfer (FRET) imaging. The activity of caspase-8 during high-fluence LPLI-induced apoptosis was studied by monitoring the cellular distribution of [Bid-CFP] reporters using fluorescence imaging. The following temporal sequence of cellular events was observed during apoptosis induced by high-fluence LPLI (120 J/cm², ASTC-a-1 cells): (1) immediate generation of mitochondrial ROS following laser irradiation, reaching a maximum level 60 min after irradiation; (2) onset of $\Delta\Psi_m$ decrease 15 min after laser irradiation, reaching a minimum level 50 min after irradiation; and (3) activation of caspase-3 between 30 min and 180 min after laser irradiation. Our results also show that the high-fluence LPLI does not activate caspase-8, indicating that the induced apoptosis was initiated directly from mitochondrial ROS generation and $\Delta\Psi_m$ decrease, independent of the caspase-8 activation.
© 2007 Society of Photo-Optical Instrumentation Engineers. [DOI: 10.1117/1.2804923]

Keywords: low-power laser irradiation (LPLI); apoptosis; caspase-3; caspase-8; fluorescence resonance energy transfer (FRET); mitochondrial membrane potential; reactive oxygen species (ROS).

Paper 06384RR received Jan. 3, 2007; revised manuscript received Jun. 20, 2007; accepted for publication Jun. 22, 2007; published online Nov. 13, 2007.

1 Introduction

Low-power laser irradiation (LPLI) can modulate various biological processes.¹ For instance, LPLI can induce cell proliferation and differentiation.^{2,3} It has been used to treat diseases with regeneration limitations⁴ and to promote wound healing.^{5,6} LPLI, in combination with a photosensitizer, can also induce apoptosis via photodynamic actions.^{7,8} High-fluence LPLI interferes with cell cycles and inhibits cell proliferation; thus, it can be used to control certain types of hyperplasia.^{9–11} Some studies suggest that LPLI has a stimu-

latory effect on cell proliferation at relatively low fluences but an inhibitory effect at high fluences.^{12,13} Furthermore, the biological effects of LPLI also depend on laser wavelength, power density, irradiation procedure, and cell type.^{14,15} Our previous studies showed that low-fluence LPLI induced proliferation of human lung adenocarcinoma cells (ASTC-a-1),¹⁶ while high fluence LPLI induced caspase-3 activation and apoptosis.¹⁷

There have been many reports on the mechanism of low-fluence LPLI-induced cell proliferation. For example, it can induce expression or activation of certain signal proteins, such as PKC (protein kinase Cs),¹⁶ ERK (extracellular signal-regulated kinase),¹⁸ Akt,¹⁹ PDGF (platelet-derived growth

Address all correspondence to Da Xing, PhD, South China Normal University, MOE Key Laboratory of Laser Life Science and Institute of Laser Life Science, Guangzhou 510631, China. Tel: +86-20-85210089; Fax: +86-20-85216052; E-mail: xingda@scnu.edu.cn

factor),²⁰ VEGF (vascular endothelial growth factor),²¹ NGF (nerve growth factor),²² CyclinD1,²² IL-8 (interleukin-8),²³ and IL-1 α (interleukin-1 alpha).²³ Low-fluence LPLI can also induce changes in reactive oxygen species (ROS) production,²⁴ Ca²⁺ concentration,²⁵ ATP quantity,²⁶ mitochondrial membrane potential ($\Delta\Psi_m$),²⁶ and intracellular pH.²⁷ However, so far there are no definitive conclusions on the mechanism of high-fluence LPLI-induced cell death.

Apoptosis is an important cellular event that plays a key role in pathology and treatment of many diseases.^{28,29} The mechanisms of initiation and regulation of apoptosis are complex and diverse. Some studies suggest that ROS generation, $\Delta\Psi_m$ decrease, and caspase activation are all involved in photodynamic therapy (PDT)-induced cell apoptosis.^{30,31} There are two main pathways to initiate and regulate cell apoptosis. One is the death receptor pathway (receptor/caspase-8/mitochondria/caspase-3), and the other is the mitochondria pathway (mitochondria/caspase-3).³²

Fluorescence resonance energy transfer (FRET) has been widely used to study protein-protein interactions in living cells.³³⁻³⁵ It can be effectively used to study cellular activities, such as caspase activation during cell apoptosis, with specifically designed genetic reporters.^{36,37}

In this study, both ASTC-a-1 cells and COS-7 cells were irradiated by a He-Ne laser under a fluence of 120 J/cm² and 80 J/cm², respectively, for a duration of 10 min in the absence of a photosensitizer to induce apoptosis. In order to study the mechanism of the induced apoptosis, we measured and analyzed the dynamics of ROS generation, change of $\Delta\Psi_m$, and activity of caspase-3 before and after the laser irradiation. In order to determine the pathway of the induced cells apoptosis, we also observed *in vivo* caspase-8 activity.

2 Materials and Methods

2.1 Cell Culture

Human lung adenocarcinoma cells (ASTC-a-1) and African green monkey SV40-transformed kidney fibroblast cells (COS-7) were grown on 22-mm culture glasses, in Dulbecco's modified Eagle's medium (DMEM, Life Technologies, Inc.), supplemented with 15% fetal bovine serum, 50 units/mL penicillin, and 50 g/mL streptomycin in 5% CO₂, 95% air at 37°C in a humidified incubator. In all experiments, 70 to 85% confluent cultures were used.

2.2 Chemicals and Plasmids

The following fluorophore probes were used: dichlorodihydrofluorescein diacetate (H₂DCFDA, 10 μ M, Molecular Probes, Inc.) to detect the generation of ROS; MitoTracker Deep Red 633 (100 nM, Molecular Probes, Inc.) to stain mitochondria; and Rhodamine 123 (5 μ M, Alexis Biochemicals, Inc.) to monitor $\Delta\Psi_m$. The cells were incubated in DMEM with different fluorophore probes. The optimal concentrations and incubation times for each of the probes were determined experimentally.

In addition, we used Lipofectin reagent (Invitrogen life Technologies, Inc.) to transfect plasmid DNA into ASTC-a-1 cells and G418 antibiotic (0.8 mg/mL, Sino-American Biotech, Inc., China) to screen the cells stably expressing reporter

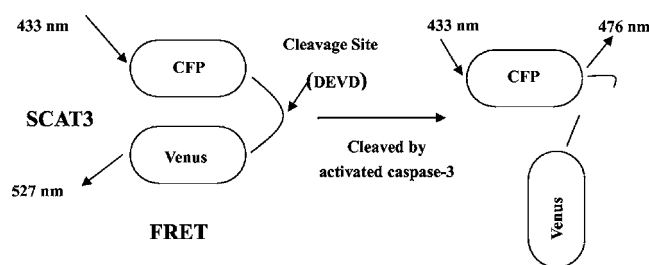


Fig. 1 The working principle of genetic reporter SCAT3. The reporter consists of a donor CFP and an acceptor Venus. The donor and the acceptor are linked with a caspase-3 recognition and cleavage sequence (DEVD). The activation of caspase-3 leads to the cleavage of the linker, thus effectively reducing the FRET.

[SCAT3]. The pSCAT3 was a gift from Dr. Masayuki Miura, and the pBid-CFP was a gift from Dr. Kazunari Taira.

2.3 Laser Irradiation of Cells

For irradiation of the ASTC-a-1 cells and COS-7 cells, a 633-nm He-Ne laser inside a confocal laser scanning microscope (LSM510-ConfoCor2, Zeiss, Jena, Germany) was used. Laser irradiation was performed through the objective lens of the microscope. In this setup, only the cells under observation were irradiated by the laser. The cells in the selected area were irradiated for 10 min with fluences of 120 J/cm² and 80 J/cm². The power dose densities of the laser on the cellular level were 200 mW/cm² and 133 mW/cm². The laser irradiation sizes were 0.025 cm² and 0.038 cm². A minitype culture chamber with CO₂ supply (Tempcontrol 37-2 Digital, Zeiss, Germany) was used in order to keep cells under normal culture conditions (37°C, 5% CO₂) during irradiation.

2.4 FRET Reporters

A genetic FRET reporter, SCAT3, was used to monitor caspase-3 activity. The working mechanism of SCAT3 is shown in Fig. 1. This reporter consists of a donor cyan fluorescent protein (CFP) and an acceptor Venus (a mutant of yellow fluorescent protein). The donor and the acceptor are linked with a caspase-3 recognition and cleavage sequence (DEVD). Activation of caspase-3 leads to the cleavage of the linker, thus effectively reducing the FRET. Therefore, a decrease in the FRET represents activation of the caspase-3.³⁶ Another genetic reporter, Bid-CFP, was used to measure the caspase-8 activity. The working mechanism of this specific reporter is shown in Fig. 2. In the plasmid Bid-CFP, CFP is fused to the C terminus of Bid. The activation of caspase-8 leads to the cleavage of the Bid protein and yields two fragments (p15 and p7). An exposed glycine residue at the C

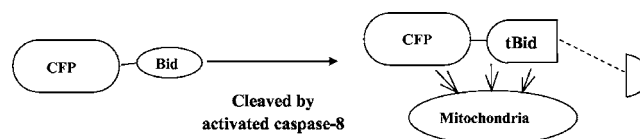


Fig. 2 The working principle of genetic reporter Bid-CFP. The reporter consists of a CFP and a Bid protein. The activation of caspase-8 leads to the cleavage of the Bid protein, causing aggregation and localization of CFP-tBid (C terminal of Bid) in the mitochondria.

terminus of Bid (tBid) undergoes N-myristoylation, and the resulting CFP-tBid is translocated to the mitochondrial outer membrane. The aggregation and localization of the CFP-tBid in mitochondria represent activation of caspase-8.³⁸ Using a genetic reporter technique based on SCAT3 and Bid-CFP, the spatiotemporal dynamics of caspase-3 and caspase-8 activity in living cells was monitored in real time during laser-irradiation-induced apoptosis.

2.5 Imaging Analysis of Living Cells

In order to image the activities of a single cell, a confocal laser scanning microscope (LSM) system was used. The system is equipped with a krypton-argon air-cooled laser (30 mW) and a He-Ne laser (5 mW) for excitation illumination. The illumination power was reduced to 3 to 0.3% of the maximum power of the excitation lasers to avoid fluorescence saturation and bleaching. Imaging was performed before and after laser irradiation, and the images were acquired with a Plan-Neofluar 40X/NA1.3 oil-immersed objective lens. Cells were maintained at 37°C, 5% CO₂ during imaging with the minitype culture chamber. For the measurement of ROS and $\Delta\Psi_m$, cells stained with H₂DCFDA and Rhodamine 123 were excited using the krypton-argon laser. The excitation wavelength was 488 nm, the beamsplitter was NFT 490 nm, and the emission detection filter was BP 500 to 550 nm. For the measurement of the *in vivo* FRET effect, cells transfected with SCAT3 were excited using the krypton-argon laser. The excitation wavelength was 458 nm, the beamsplitter was NFT 515 nm, and the emission detection filters were BP 470 to 500 nm and LP 530 nm for emissions of CFP and Venus, respectively. For the measurement of caspase-8 activity and the mitochondria staining, cells transfected with Bid-CFP and stained with MitoTracker Deep Red were excited by the krypton-argon laser and the He-Ne laser. The wavelengths used were 458 nm for the excitation of CFP and 633 nm for the excitation of MitoTracker Deep Red. The beamsplitter was NFT 635 nm, and the emission detection filters were BP 470 to 500 nm and LP 650 nm for the emissions of CFP and MitoTracker Deep Red, respectively. For intracellular measurements, the desired measurement area was chosen in the LSM image. To quantify the results, the fluorescence emission intensities were obtained with Zeiss Rel3.2 image processing software (Zeiss, Jena, Germany). All imaging experiments were repeated in different cells. For the analysis of Bid-CFP translocation, images were analyzed with MATLAB 6.5 by drawing regions around individual cells and then computing the SD of the intensity of the pixels (punctuate/diffuse) and integrated brightness (total brightness). All imaging experiments were repeated in different cells. As a rough indication of the range of variability among cells within an experiment, error bars show the SD.

3 Results

3.1 High-Fluence LPLI-Induced Mitochondrial ROS Generation

The generation of ROS in ASTC-a-1 cells by high-fluence LPLI (120 J/cm²) was monitored by measuring changes in fluorescence resulting from the oxidation of intracellular H₂DCFDA (nonfluorescent) to DCF (fluorescent). Cells were

incubated with 10- μ M H₂DCFDA for 30 min in DMEM culture liquid in an incubator. Fluorescence progressively increased after the cells were irradiated, indicating the generation of ROS. The typical time-course images of cells loaded with H₂DCFDA after laser irradiation are shown in Fig. 3(a). The average fluorescence intensity of DCF after high-fluence LPLI from five different cells is shown in Fig. 3(b). The DCF fluorescence was observed as soon as the laser irradiation was completed, while there was a low level of detectable DCF fluorescence before irradiation corresponding to the ROS level in rest cells (data not shown). This result indicated an immediate generation of ROS following the laser irradiation. This was followed by a gradual increase of DCF fluorescence intensity. About 60 min after laser irradiation, the DCF fluorescence intensity reached a plateau [Figs. 3(a) and 3(b)]. In order to determine whether this phenomenon happened in other apoptosis doses, we used 80 J/cm² LPLI to irradiate ASTC-a-1 cells; the result then showed that at 100 min after laser irradiation, the DCF fluorescence intensity reached a plateau [Figs. 3(a) and 3(b)]. Similar results were also obtained in COS-7 cells [Fig. 3(c)].

To confirm that the increased DCF fluorescence after laser irradiation originated from mitochondria, ASTC-a-1 cells were coloaded with MitoTracker Deep Red 633, a mitochondria-specific dye. The perinuclear fluorescence of DCF from the cells colocalized with MitoTracker Deep Red is shown in Fig. 3(d). The overlaid images of the DCF fluorescence and MitoTracker Deep Red fluorescence indicate that ROS were mostly formed in mitochondria. Similar results were also obtained in COS-7 cells (data not shown).

3.2 High-Fluence LPLI-Induced Mitochondrial Membrane Potential ($\Delta\Psi_m$) Decrease

ASTC-a-1 cells were loaded with Rhodamine 123 dyes in order to monitor $\Delta\Psi_m$ in single cells by confocal laser scanning microscopy. Polarized mitochondria would appear as bright fluorescent spheres; thus, a reduction in fluorescence would indicate the decrease of $\Delta\Psi_m$. The typical time-course images of cells loaded with Rhodamine 123 after laser irradiation are shown in Fig. 4(a). The average fluorescence intensities of Rhodamine 123 at different times after the high-fluence LPLI from five different cells are shown in Fig. 4(b). About 15 min after laser irradiation, the fluorescence intensity started to decrease [Fig. 4(b)], which indicated the decrease of $\Delta\Psi_m$. About 50 min after laser irradiation, the fluorescence intensity reached the lowest level. Without laser treatment, $\Delta\Psi_m$ was nearly unchanged, as shown by the control data in Fig. 4(b). Comparing Fig. 3(b) with Fig. 4(b), it is apparent that the generation of mitochondrial ROS (immediately following laser irradiation) precedes the decrease of $\Delta\Psi_m$ (15 min after irradiation). The results suggest that the ROS production under high-fluence LPLI might have caused the $\Delta\Psi_m$ decrease. Similar results were also obtained in COS-7 cells [Fig. 4(c)].

3.3 High-Fluence LPLI-Activated Caspase-3

FRET imaging was used to determine the dynamic changes of caspase-3 in ASTC-a-1 cells transfected by SCAT3 reporters after high-fluence LPLI (120 J/cm²). The typical time-course Venus/CFP ratio images of cells stably expressing SCAT3 re-

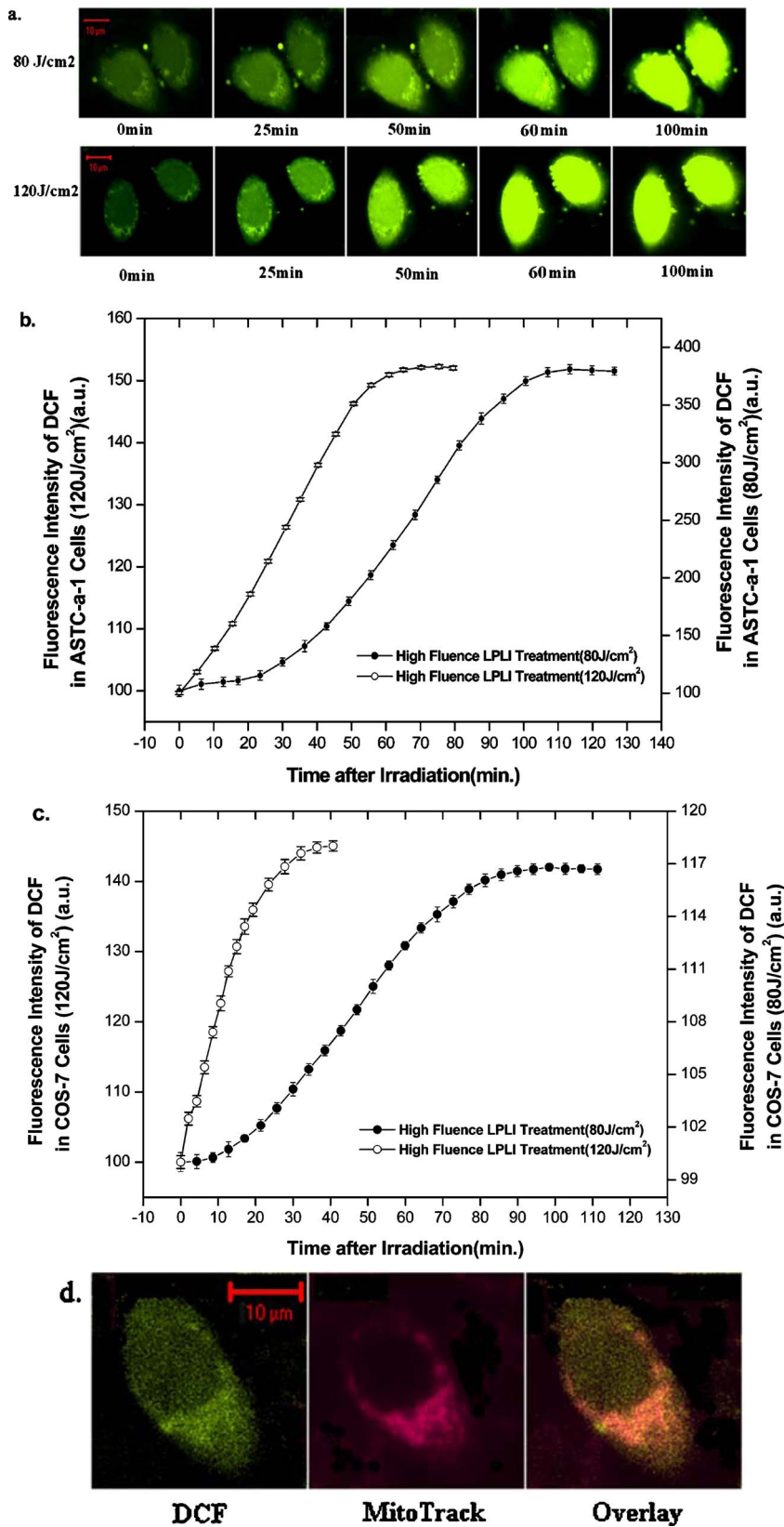


Fig. 3 Generation of mitochondrial ROS by high-fluence LPLI (120 J/cm² and 80 J/cm²). Cells loaded with the H₂DCFDA and MitoTracker Deep Red 633 probes were irradiated and imaged (exe. 488 nm, em. BP 500 to 550 nm for DCF; exe. 633 nm, em. LP 650 nm for MitoTracker Deep Red 633). The time after laser irradiation is indicated in each panel. Bar=10 μm. (a) The typical time-course images of ASTC-a-1 cells. (b) The fluorescence intensity curve of DCF (*n*=5) with the standard deviations as the error bars in ASTC-a-1 cells. (c) The fluorescence intensity curve of DCF (*n*=5) with the standard deviations as the error bars in COS-7 cells. (d) The overlaid fluorescence images of DCF and MitoTracker Deep Red 633 in ASTC-a-1 cells.

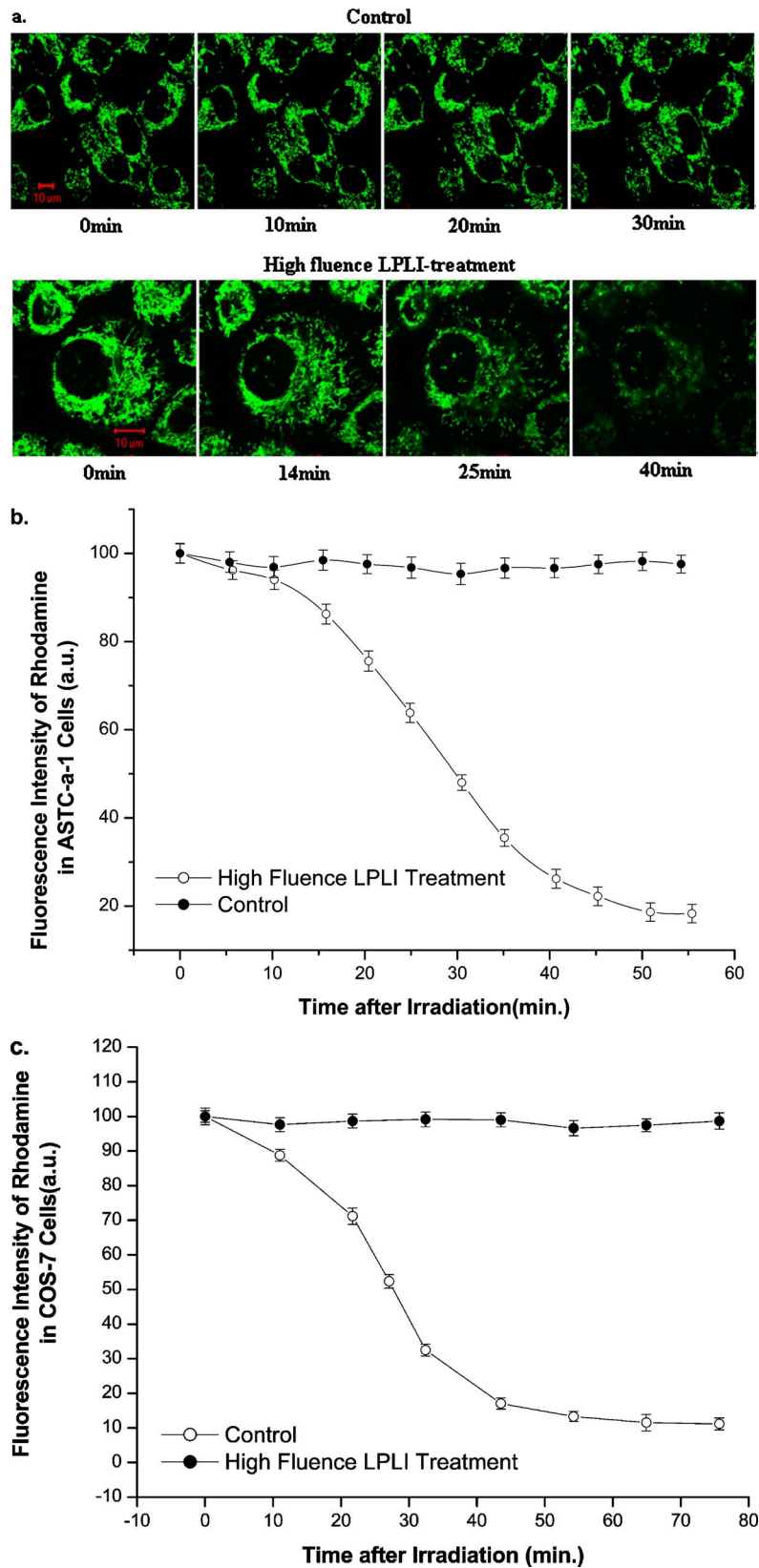


Fig. 4 Changes of $\Delta\Psi_m$ induced by high-fluence LPLI (120 J/cm^2). Cells loaded with the Rhodamine 123 probe were irradiated and imaged (exc. 488 nm, em. BP 500 to 550 nm). The time after laser irradiation is indicated in each panel. Bar= $10 \mu\text{m}$. (a) The typical time-course images of ASTC-a-1 cells. (b) The fluorescence intensity of Rhodamine 123 ($n=5$) with the standard deviations as the error bars in ASTC-a-1 cells. (c) The fluorescence intensity of Rhodamine 123 ($n=5$) with the standard deviations as the error bars in COS-7 cells.

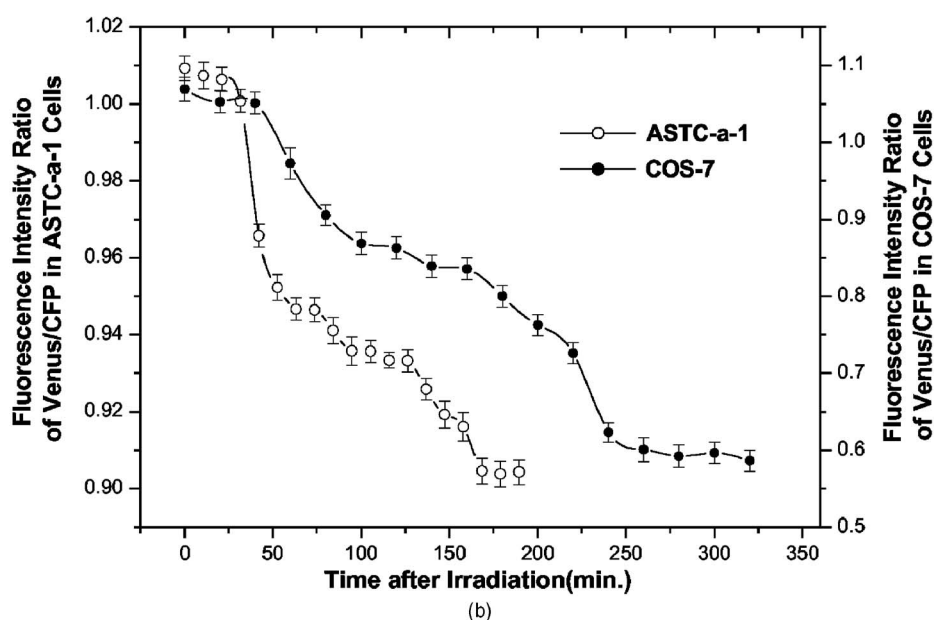
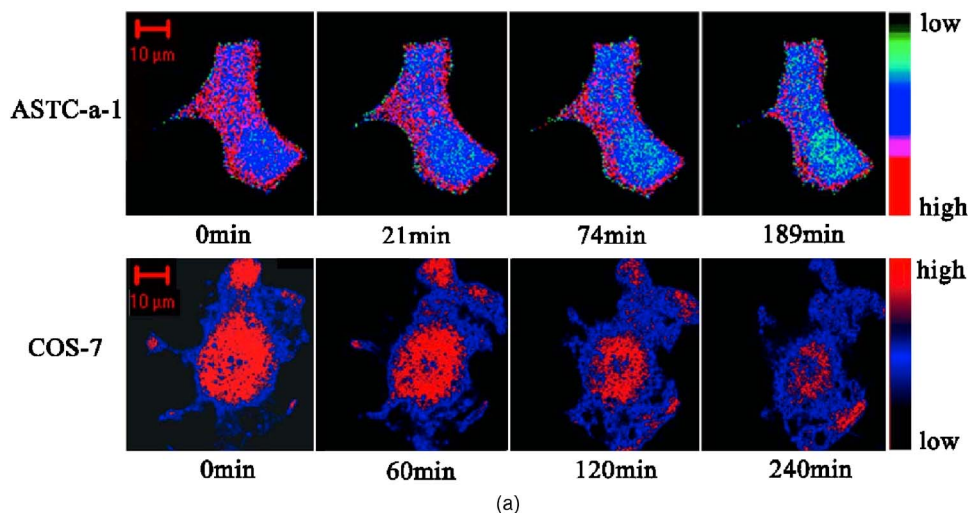


Fig. 5 Dynamics of caspase-3 activation in response to high-fluence LPLI (120 J/cm^2). Cells stably expressing SCAT-3 were irradiated and imaged (exe. 458 nm, em. BP 470 to 500 nm for CFP, LP 530 nm for Venus). The time after the irradiation is indicated in each panel. Bar= $10 \mu\text{m}$. (a) The typical time-course pseudocolor fluorescence images of Venus/CFP of ASTC-a-1 cells and COS-7 cells. (b) The fluorescence intensity curve of Venus/CFP ratio ($n=5$) with the standard deviations as the error bars in ASTC-a-1 cells and COS-7 cells.

porters after LPLI show an intensity decrease in Fig. 5(a) (top). The average emission ratio of Venus/CFP from five different cells is plotted as function of time during laser irradiation [Fig. 5(b)]. The fluorescence intensities of Venus/CFP first decreased slightly during the first 30 min after LPLI then decreased significantly. About 3 h after laser irradiation, the fluorescence intensity from the cells reached a low, stable level. These results indicated that the caspase-3 activity increased gradually due to laser irradiation, noticeably 30 min after irradiation. Comparing Fig. 4(b) with Fig. 5(b), it is clear that the onset of $\Delta\Psi_m$ decrease (15 min after irradiation) precedes that of caspase-3 activation (30 min after irradiation). The results suggest that the $\Delta\Psi_m$ decrease might affect the activity of caspase-3. The similar results were also obtained in COS-7 cells [Figs. 5(a) and 5(b)].

3.4 Effect of High-Fluence LPLI on Caspase-8

In order to determine the pathway of cell apoptosis induced by high-fluence LPLI (120 J/cm^2), caspase-8 activity was observed using the fluorescence of the Bid-CFP reporter, because aggregation and localization of Bid-CFP in mitochondria would represent the activation of caspase-8.³⁸ The typical time-course images of ASTC-a-1 cells transfected with pBid-CFP reporters after laser irradiation are shown in Fig. 6(a) (top). The Bid-CFP punctuate/diffuse index at different times after the high-fluence LPLI from five different cells is shown in Fig. 6(c). The Bid-CFP fluorescence was distributed evenly in the cytoplasm, and no aggregation occurred, even after apoptosis. To determine the location of Bid-CFP, the cells transfected with pBid-CFP were also loaded with MitoTracker

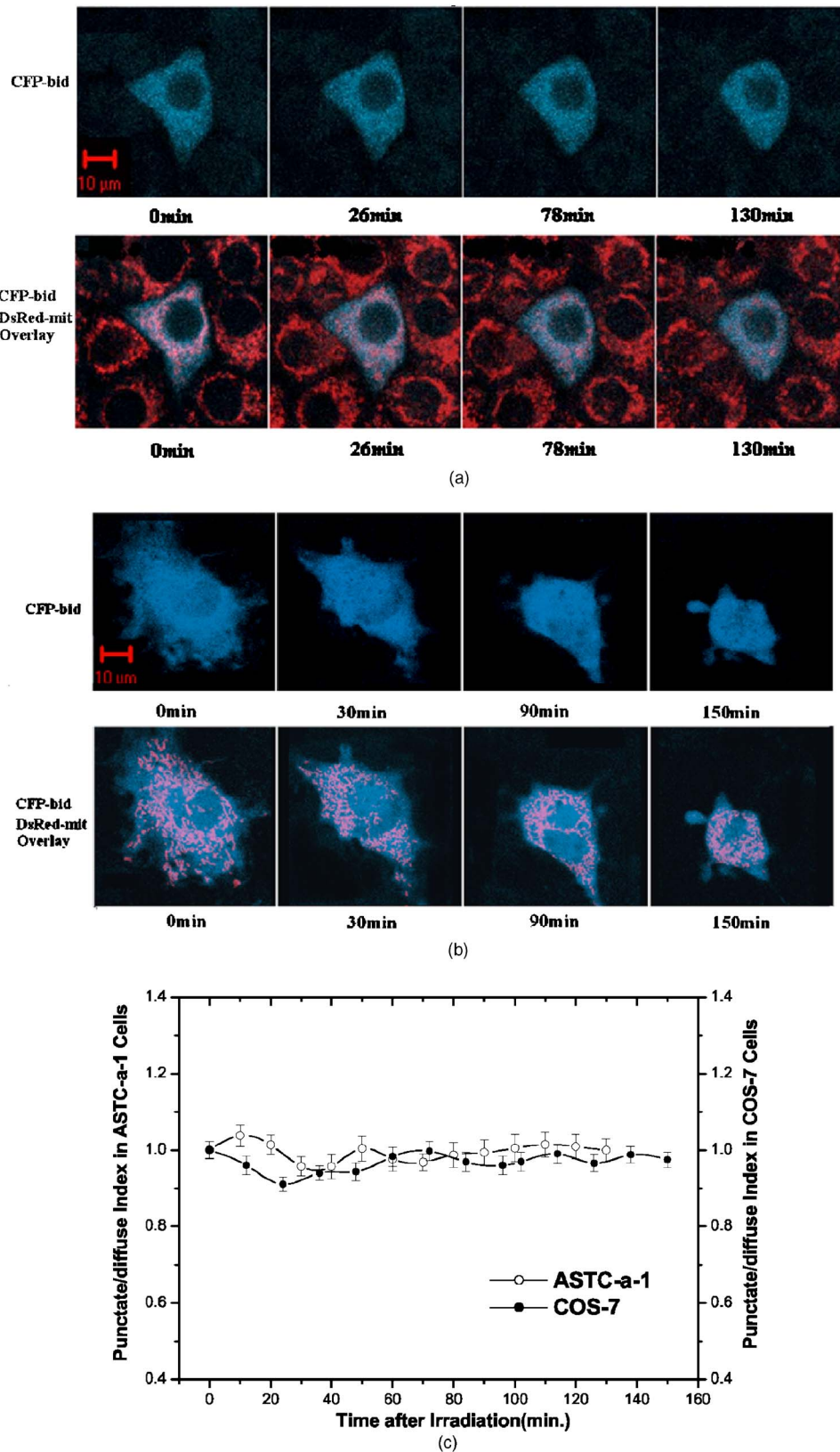


Fig. 6 Effect of high-fluence LPLI (120 J/cm²) on caspase-8. Cells transfected with Bid-CFP were stained by MitoTracker Deep Red 633 and were irradiated and imaged (exe. 458 nm, em. BP 470 to 500 nm for Bid-CFP; exe. 633 nm, em. LP 650 nm for MitoTracker Deep Red 633). The time after high-fluence LPLI is indicated in each panel. Bar=10 μ m. (a) The typical time-course images of Bid-CFP in ASTC-a-1 cells (top). The typical time-course overlaid images of Bid-CFP and MitoTracker Deep Red 633 in ASTC-a-1 cells (bottom). (b) The typical time-course images of Bid-CFP in COS-7 cells (top). The typical time-course overlaid images of Bid-CFP and MitoTracker Deep Red 633 in COS-7 cells (bottom). (c) Bid-CFP punctate/diffuse index of ASTC-a-1 and COS-7 cells at different times after the high fluence LPLI (n=5 for each cell line).

Deep Red. The time-course fluorescence images of MitoTracker Deep Red overlaid with images of pBid-CFP are shown in Fig. 6(a) (bottom). There was no colocalization. These results demonstrate that caspase-8 was not activated by the high-fluence LPLI, suggesting that high-fluence LPLI-induced apoptosis was initiated directly from the mitochondria pathway, independent of the activity of caspase-8. Similar results were also obtained in COS-7 cells [Figs. 6(b) and 6(c)].

4 Discussion

The mechanism of low-fluence LPLI-induced cell proliferation has been reported in various studies, but the mechanism of high-fluence LPLI-induced cell death remains unclear. This study is an attempt to understand the mechanism of cell apoptosis induced by high-fluence LPLI, by investigating a cascade of phenomena induced by laser irradiation of ASTC-1-a cells. Cellular functions such as generation of ROS and change of $\Delta\Psi_m$ were studied using fluorescent-vital probes. Caspase-3 and caspase-8 activities were monitored in real time in single living cells using genetic reporters.

In our studies, we chose two cell lines, ASTC-a-1 and COS-7, to study the mechanism of high-fluence LPLI induced cell apoptosis. The former were human lung adenocarcinoma cells; hence, our results could be applied to cancer therapy. The latter, although transformed with SV40, were not cancer cells and did not have multiple oncogene activation; hence, our results should be more applicable to the normal cells that were in tissues treated with LPLI.

Our previous work shows that lower-fluence LPLI can promote ASTC-a-1 proliferation at a dose of 0.5 to 0.8 J/cm² (Ref. 16), and high fluence LPLI can induce ASTC-a-1 apoptosis at the dose 60 to 120 J/cm². In this study, we choose 120 J/cm² as the major stimulation dose and 80 J/cm² as the parallel dose. We found that both doses of LPLI cause similar biological effects, and the difference is major in the initiate time and end time of these cellular events, mentioned earlier.¹⁷

In PDT-induced apoptosis, there is evidence that ROS plays an important role during the progression of apoptosis.³⁰ One of the objectives of this study was to detect the generation of ROS as a result of high-fluence LPLI. Our results show an immediate mitochondrial ROS generation induced by the laser irradiation, followed by a gradual increase of ROS, as indicated by the increase of DCF fluorescence intensity (see Fig. 3) from irradiated cells containing H₂DCFDA. This observation agrees with the suggestions that the initial ROS, such as ¹O₂, O₂, and H₂O₂, are produced as a result of light absorption either by endogenous porphyrins or cytochrome in mitochondria. We suggest that endogenous porphyrins may play a role based on the increase of cellular ROS levels after higher-fluence LPLI (Fig. 3). Following are three examples:

1. Cytochrome C oxidase, the terminal enzyme of the respiratory chain, can be involved as photoacceptors.³⁹⁻⁴²

2. After light absorption, oxidative stress induces the redox activity of respiratory chain acceleration, resulting in a massive production of ROS.^{43,44}

3. Low-fluence LPLI can also induce the mitochondrial ROS generation, but the difference is the relative low level compared with the high level induced by high-fluence LPLI.²⁷

The decrease of the mitochondrial membrane potential, $\Delta\Psi_m$, may promote inner membrane permeabilization, disrupt the mitochondria structure, and cause the release of proapoptotic factors. In our study, 15 min after laser irradiation, the decrease in $\Delta\Psi_m$ began, as indicated by Rhodamine fluorescence intensity in irradiated cells [Fig. 4(a)].

The release of proapoptotic factors, such as cytochrome C, can activate caspase-9, and subsequently, caspase-3. Utilizing the FRET, we found that the caspase-3 activity in ASTC-a-1 cells increased gradually after high-fluence LPLI, as indicated by the decrease of the fluorescence intensity ratio of Venus/CFP from the cells transfected by SCAT3, as shown in Fig. 5.

Caspase-8 activity was studied in order to determine whether high-fluence LPLI-induced cell apoptosis was initiated directly from the mitochondria pathway or mediated by upstream caspase-8. Figure 6 shows that the fluorescence from Bid-CFP in irradiated cells was uniformly distributed in the cytoplasm without aggregation in the mitochondria. Therefore, caspase-8 was not activated by high-fluence LPLI, which indicates that high-fluence LPLI-induced cell apoptosis was initiated directly from the mitochondria pathway, independent of caspase-8. This observation explains why high-fluence LPLI-induced caspase-3 activation is a relatively earlier event [about 30 min after laser irradiation, Fig. 5(b)], compared with the TNF- α -induced apoptosis (about 2 h after TNF- α treatment), which was mediated by the caspase-8.⁴⁵

Our experimental results in Figs. 3(b), 4(b), and 5(b) show a clear cascade of cellular events during high-fluence LPLI-induced apoptosis:

1. Immediate generation of mitochondrial ROS following laser irradiation, reaching a maximum level 60 min after irradiation.

2. Onset of $\Delta\Psi_m$ decrease 15 min after laser irradiation, reaching a minimum level 50 min after irradiation.

3. Activation of caspase-3 between 30 min and 180 min after laser irradiation.

Therefore, we propose that the cellular responses to laser irradiation follow a temporal sequence shown as follows: Without evidence of caspase-8 activation in our experiments, we conclude that light is absorbed directly by endogenous porphyrins in mitochondria, resulting in the initial ROS generation. And we found that both ASTC-a-1 cells and COS-7 cells can be induced by the increase of mitochondrial ROS. Therefore, the porphyrin may exist not only in ASTC-a-1 cells but also in many cell lines.²⁷ Interestingly, we found that at a fluence of 120 J/cm², the mitochondrial ROS level in COS-7 cells reaches the plateau much more quickly (40 min) than in ASTC-a-1 cells (60 min). This result indicates that COS-7 cells are more sensitive to light than ASTC-a-1 cells, although the distinction is insignificant [Figs. 3(b) and 3(c)]. After light absorption, oxidative stress induces the redox activity of respiratory chain acceleration, resulting in massive production of ROS. Subsequently, the generation of ROS induces the decrease of $\Delta\Psi_m$ and inner membrane permeabilization, thereby promoting mitochondrial structure destruction and causing the release of proapoptotic factor. The release of proapoptotic factors, such as cytochrome C, activates the caspase-9, and subsequently, caspase-3, which finally results in apoptosis.

In conclusion, our experimental results show that the mitochondrial ROS generation, the decrease of $\Delta\Psi_m$, and the activation of caspase-3, in that order, play a critical role in the high-fluence LPLI-induced ASTC-a-1 cell apoptosis. To our best knowledge, this is the first time that the temporal sequence of cellular activities during high-fluence LPLI-induced apoptosis has been unequivocally determined using fluorescence imaging techniques. Our study contributes to the understanding of the mechanism of LPLI-induced biological responses. In addition, this research would be useful due to the fact that high fluences producing cell death by apoptosis may explain some of the negative findings in LPLI studies where too high a fluence may have been inadvertently used.

Acknowledgments

The authors thank Dr. Masayuki Miura for providing pSCAT3 and Dr. Kazunari Taira for providing pBid-CFP. This research is supported in part by the National Natural Science Foundation of China (Contract Grant Nos. 60378043, 30470494), by the Natural Science Foundation of Guangdong Province (Contract Grant Nos. 015012, 04010394), and by a grant from the U.S. National Institute of Health (Grant No. P20 RR016478 from the INBRE Program of the National Center for Research Resources).

References

1. T. Karu, "Photobiology of low-power laser effects," *Health Phys.* **56**, 691–704 (1989).
2. B. D. Nadav, S. Gaviella, I. Andrey, W. Anton, O. Uri, and H. Orna, "Low-energy laser irradiation affects satellite cell proliferation and differentiation *in vitro*," *Biochim. Biophys. Acta* **1448**, 372–380 (1999).
3. C. T. Jui and C. K. Ming, "The biological effects of low power laser irradiation on cultivated rat glial and glioma cells," *J. Clin. Laser Med. Surg.* **9**, 35–41 (1991).
4. M. Khadra, N. Kasem, H. R. Haanaes, J. E. Ellingsen, and S. P. Lyngstadaas, "Enhancement of bone formation in rat calvarial bone defects using low-level laser therapy," *Oral Surg. Oral Med. Oral Pathol. Oral Radiol. Endod.* **97**, 693–700 (2004).
5. M. S. Ribeiro, D. D. Da Silva, C. E. De Araujo, S. F. De Oliveira, C. M. Pelegrini, T. M. Zorn, and D. M. Zezell, "Effects of low-intensity polarized visible laser radiation on skin burns: a light microscopy study," *J. Clin. Laser Med. Surg.* **22**, 59–66 (2004).
6. J. S. Kawalec, V. J. Hetherington, T. C. Pfennigwerth, D. S. Dockery, and M. Dolce, "Effect of a diode laser on wound healing by using diabetic and nondiabetic mice," *J. Foot Ankle Surg.* **43**, 214–220 (2004).
7. T. Kaneko, H. Chiba, T. Yasuda, and K. Kusama, "Immune activation and chronic inflammation as the cause of malignancy in oral lichen planus: is there any evidence?," *Oral Oncol.* **40**, 787–792 (2004).
8. C. Abels, "Targeting of the vascular system of solid tumors by photodynamic therapy (PDT)," *Photochem. Photobiol. Sci.* **3**, 765–771 (2004).
9. S. O. Kane, T. D. Shields, W. S. Gilmore, and J. Allen, "Low intensity laser irradiation inhibits tritiated thymidine incorporation in the hemopoietic cell lines HL-60 and U937," *Lasers Surg. Med.* **14**, 34–39 (1994).
10. A. J. Gross and W. Jelkmann, "Helium-neon laser irradiation inhibits the growth of kidney epithelial cells in culture," *Lasers Surg. Med.* **10**, 40–44 (1990).
11. J. M. Ocaña-Quero, J. Perez de la Lastra, R. Gomez-Villamandos, and M. Moreno-Millán, "Biological effect of helium-neon (He-Ne) laser irradiation on mouse myeloma (sp2-ag14) cell line *in vitro*," *Lasers Med. Sci.* **13**, 214–218 (1998).
12. R. Lubart, Y. Wollman, H. Friedmann, S. Rochkind, and I. Lanlicht, "Effects of visible and near-infrared lasers on cell cultures," *J. Photochem. Photobiol., B* **12**, 305–310 (1992).
13. T. Karu, "Effects of visible radiation on cultured cells," *Photochem. Photobiol.* **52**, 1089–1089 (1990).
14. A. D. Meyers, J. Joyce, and J. J. Cohen, "Effects of low-watt helium neon laser radiation on human lymphocyte cultures," *Lasers Surg. Med.* **6**, 540–542 (1987).
15. J. A. Morales, M. J. Ruiz-Gomez, L. Gil-Carmona, A. Souviron, and M. Martinez-Morillo, "He-Ne laser has no effect on cell cycle phases of human colon adenocarcinoma cells," *Rev. Esp. Fisiol.* **51**, 43–47 (1995).
16. X. J. Ago, T. S. Chen, D. Xing, F. Wang, Y. H. Pei, and X. B. Wei, "Single cell analysis of PKC activation during proliferation and apoptosis induced by laser irradiation," *J. Cell Physiol.* **206**, 441–448 (2005).
17. F. Wang, T. S. Chen, D. Xing, J. J. Wang, and Y. X. Wu, "Measuring dynamics of caspase-3 activity in living cells using FRET technique during apoptosis induced by high fluence low-power laser irradiation," *Lasers Surg. Med.* **36**, 2–7 (2005).
18. G. Shefer, U. Oron, A. Irintchev, A. Wernig, and O. Halevy, "Skeletal muscle cell activation by low-energy laser irradiation: a role for the MAPK/ERK pathway," *J. Cell Physiol.* **187**, 73–80 (2001).
19. G. Shefer, I. Barash, U. Oron, and O. Halevy, "Low-energy laser irradiation enhances *de novo* protein synthesis via its effects on translation-regulatory protein in skeletal muscle myoblasts," *Biochim. Biophys. Acta* **1593**, 131–139 (2003).
20. W. Yu, J. O. Naim, and R. J. Lanzafame, "The effect of photoirradiation on the secretion of TGF- β PDGF and bFGF from fibroblasts *in vitro*," *Lasers Surg. Med. Suppl.* **6**, 8–8 (1994).
21. N. Kipshidze, V. Nikolaychik, M. H. Keelan, L. R. Shankar, A. Khanna, R. Kornowski, M. Leon, and J. Moses, "Low-power helium: neon laser irradiation enhances production of vascular endothelial growth factor and promotes growth of endothelial cells *in vitro*," *Lasers Surg. Med.* **28**, 355–364 (2001).
22. F. Schwartz, C. Brodie, E. Appel, G. Kazimirsky, and A. Shainberg, "Effect of helium/neon laser irradiation on nerve growth factor synthesis and secretion in skeletal muscle cultures," *J. Photochem. Photobiol., B* **66**, 195–200 (2002).
23. H. S. Yu, K. L. Chang, C. L. Yu, J. W. Chen, and G. S. Chen, "Low-energy helium-neon laser irradiation stimulates interleukin-1 alpha and interleukin-8 release from cultured human keratinocytes," *J. Invest. Dermatol.* **107**, 593–596 (1996).
24. N. Grossman, N. Schneid, H. Reuveni, S. Halevy, and R. Lubart, "780 nm low power diode laser irradiation stimulates proliferation of keratinocyte cultures: involvement of reactive oxygen species," *Lasers Surg. Med.* **22**, 212–218 (1998).
25. T. Karu, N. Smolyaninova, and A. Zelenin, "Long-term and short-term response of human lymphocytes to He-Ne laser radiation," *Lasers Life Sci.* **4**, 167–178 (1991).
26. S. Passarella, E. Casamassima, S. Molinari, D. Pastore, E. Quagliarello, I. M. Catalano, and A. Cingolani, "Increase of proton electrochemical potential and ATP synthesis in rat liver mitochondria irradiated *in vitro* by helium-neon laser," *Fed. Eur. Biochem. Soc. Lett.* **175**, 95–99 (1984).
27. E. Alexandratou, Y. Dido, H. Panagiotis, K. Dimitris, and L. Spyros, "Human fibroblast alteration induced by low power laser irradiation at the single cell level using confocal microscopy," *Photochem. Photobiol. Sci.* **1**, 547–552 (2002).
28. A. Ashkenazi and V. M. Dixit, "Death receptors: signaling and modulation," *Science* **281**, 1305–1308 (1998).
29. S. Nagata, "Apoptosis by death factor," *Cell* **88**, 355–365 (1997).
30. M. Lam, N. L. Oleinick, and A. L. Nieminen, "Photodynamic therapy-induced apoptosis in epidermal carcinoma cells. Reactive oxygen species and mitochondrial inner membrane permeabilization," *J. Biol. Chem.* **276**, 47379–47386 (2001).
31. H. Takahashi, Y. Itoh, Y. Miyauchi, S. Nakajima, I. Sakata, A. Ishida-Yamamoto, and H. Iizuka, "Activation of two caspase cascades, caspase 8/3/6 and caspase 9/3/6, during photodynamic therapy using a novel photosensitizer, ATXS10 (Na), in normal human keratinocytes," *Arch. Dermatol. Res.* **295**, 242–248 (2003).
32. D. R. Green, "Apoptotic pathways: paper wraps stone blunts scissors," *Cell* **102**, 1–4 (2000).
33. S. Fields and O. Song, "A novel genetic system to detect protein-protein interactions," *Nature (London)* **340**, 245–246 (1989).
34. B. A. Pollok and R. Heim, "Genetic instability and darwinian selection in tumors," *Trends Cell Biol.* **9**, 57–60 (1999).
35. F. Gaits and K. Hahn, "Shedding light on cell signaling: interpretation of FRET biosensors," *Sci. STKE* **3**, 1–5 (2003).
36. K. Takemoto, T. Nagai, A. Miyawaki, and M. Miura,

- “Spatio-temporal activation of caspase revealed by indicator that is insensitive to environmental effects,” *J. Cell Biol.* **160**, 235–243 (2003).
37. Y. X. Wu, D. Xing, S. M. Lou, Y. H. Tang, and Q. Chen, “Detection of caspase-3 activation in single cells by fluorescence resonance energy transfer during photodynamic therapy induced apoptosis,” *Cancer Lett.* **235**, 239–247 (2006).
 38. R. Onuki, A. Nagasaki, H. Kawasaki, T. Baba, T. Q. P. Uyeda, and K. Taira, “Confirmation by FRET in individual living cells of the absence of significant amyloid β -mediated caspase 8 activation,” *Proc. Natl. Acad. Sci. U.S.A.* **99**, 14716–14721 (2002).
 39. T. Karu, L. Pyatibrat, S. Kolyakov, and N. Afanasyeva, “Absorption measurements of a cell monolayer relevant to phototherapy: reduction of cytochrome c oxidase under near IR radiation,” *J. Photochem. Photobiol., B* **81**, 98–106 (2005).
 40. T. Karu, L. Pyatibrat, and N. Afanasyeva, “Cellular effects of low power laser therapy can be mediated by nitric oxide,” *Lasers Surg. Med.* **36**, 307–314 (2005).
 41. T. Karu, L. Pyatibrat, and G. Kalendo, “Photobiological modulation of cell attachment via cytochrome c oxidase,” *Photochem. Photobiol. Sci.* **3**, 211–216 (2004).
 42. T. Karu, L. Pyatibrat, and N. Afanasyeva, “A novel mitochondrial signaling pathway activated by visible-to-near infrared radiation,” *Photochem. Photobiol.* **80**, 366–372 (2004).
 43. D. Pastore, M. Greco, and S. Passarella, “Specific He–Ne laser sensitivity of the purified cytochrome c oxidase,” *Int. J. Radiat. Biol.* **76**, 863–870 (2000).
 44. H. Friedmann, R. Lubart, I. Laulicht, and S. J. Rochkind, “A possible explanation of laser-induced stimulation and damage of cell cultures,” *J. Photochem. Photobiol., B* **11**, 87–91 (1991).
 45. K. Q. Luo, V. C. Yu, Y. M. Pu, and D. C. Chang, “Measuring dynamics of caspase-8 activation in a single living HeLa cell during TNF alpha-induced apoptosis,” *Biochem. Biophys. Res. Commun.* **304**(2), 217–222 (2003).